3D high frame rate flow measurement using a prototype matrix transducer for carotid imaging

Fool, Fabian; Vos, Hendrik J.; Shabanimotlagh, Maysam; Soozande, Mehdi; Mozaffarzadeh, Moein; Kim, Taehoon; Kang, Eunchul; Pertijs, Michiel; Jong, Nico De; Verweij, Martin D.

DOI
10.1109/ULTSYM.2019.8925780

Publication date
2019

Document Version
Final published version

Published in
2019 IEEE International Ultrasonics Symposium, IUS 2019

2019 IEEE International Ultrasonics Symposium (IUS)
Glasgow, Scotland, October 6-9, 2019

3D high frame rate flow measurement using a prototype matrix transducer for carotid imaging

Fabian Fool[1], Hendrik J. Vos[2,1], Maysam Shabanimotlagh[1], Mehdi Soozande[2], Moein Mozaffarzadeh[1], Taehoon Kim[3], Eunchul Kang[3], Michiel Pertijs[3], Nico de Jong[1,2] and Martin D. Verweij[1,2]
[1]Acoustical Wavefield Imaging, Imaging Physics, Delft University of Technology, Delft, the Netherlands
[2]Biomedical Engineering, Thorax Center, Erasmus MC, Rotterdam, the Netherlands
[3]Electronic Instrumentation Laboratory, Delft University of Technology, Delft, the Netherlands
Email: F.Fool@tudelft.nl

***Abstract*—To accurately investigate the state of the carotid artery by the local haemodynamics and motion of the plaque using ultrasound, high-frame rate volumetric imaging is necessary. We have specifically designed a matrix array for this purpose. In this proceeding we will focus on imaging a volumetric flow profile using this matrix. For this purpose, we extend a fast frequency domain vector flow imaging method to 3D and perform measurements on a flow phantom. The results indicate that it is feasible to estimate 3D velocity vectors on a 3D grid using our matrix transducer and the proposed algorithm.**

***Index Terms*—Matrix array, Fourier domain algorithm, Vector velocity imaging, Volumetric flow, Plane wave imaging**

I. Introduction

Carotid artery disease is known to be related to coronary artery disease [1]. Since the carotid arteries can be assessed with ultrasound much better than the coronary arteries of the heart, this opens new ways of early screening for risk factors, diagnosis and treatment of cardiovascular disease. The local haemodynamics and motion of the plaque might provide a good way to assess the state of the carotid artery [2]. However, to accurately measure these phenomena using ultrasound, high-frame rate volumetric imaging is necessary [3], [4]. There are several challenges involved in making this possible, including the development of a matrix transducer that can image a volume at a high frame rate and fast algorithms to process the received data and extract the necessary parameters.

Nowadays several types of matrix transducers exist that can make volumetric images, including sparse arrays [5] and row-column arrays [6]. We have developed an alternative matrix array designed for imaging the carotid bifurcation that is build directly on top of an ASIC [7]. This matrix has a single input and output per row. Due to this implementation our matrix array operates like an electronically translatable linear array.

To quickly process the received volumetric data, algorithms with a low complexity are needed. This can be provided by Fourier domain algorithms. As an example, for beamforming plane wave data Lu's Fourier domain remapping algorithm is able to provide a lower complexity than a Delay-And-Sum(DAS) algorithm [8], [9]. For vector velocity imaging Fourier domain algorithms are also able to provide a lower complexity as has been shown by Lenge *et al.* [10]. This algorithm has shown to be 50 times more computationally efficient than a cross-correlation based estimator in 2D. We expect that in 3D this difference will be even larger, but a 3D implementation does not exist yet.

In this proceeding we will focus on imaging a volumetric flow profile using our matrix transducer. For this purpose, we will extend a fast frequency domain vector flow imaging method to 3D and perform measurements on a flow phantom.

II. Flow estimation algorithm

The 2D flow estimation algorithm by Lenge *et al.* estimates the velocities sequentially [10], i.e. by first estimating the axial velocity and then estimating the lateral velocity. This approach is however unnecessary as the velocity vectors can also be estimated directly as demonstrated by Stone *et al.* [11]. Furthermore, By using this implementation the maximum measurable displacement between successive images can be decoupled from the grid step.

The focus of Stone *et al.* is to accurately estimate a 2D displacement in case of aliasing due to spatially undersampled images. The same approach can also be applied to 3D motion estimation in ultrasound, and with a modification to the choice of frequencies this approach will also be able to track large displacements, i.e. larger than the grid stepping. In the section below we describe the algorithm and next we discuss the choice of frequencies.

A. Derivation

The core of the algorithm is the Fourier Shift theorem which states that the phase difference between two translated images is

$$\Delta\phi\left(k_x, k_y, k_z\right) = k_x\Delta x + k_y\Delta y + k_z\Delta z, \tag{1}$$

where $k_x,\ k_y,\ k_z$ are the spatial frequencies and $\Delta x,\ \Delta y,\ \Delta z$ the displacements between the images in all three directions. When putting all combinations of spatial frequencies into one expression equation (1) can be written in matrix form as

$$\Delta\vec{\phi} = K\Delta\vec{r}, \tag{2}$$

where $\Delta\vec{\phi}$ is a vector containing the phase differences for all combinations of (k_x, k_y, k_z), K a matrix containing one combination of (k_x, k_y, k_z) per row and $\Delta\vec{r}$ is a vector containing the displacements. Equation (2) indicates that the

978-1-7281-4596-9/19/$31.00 ©2019 IEEE

phase difference for every combination of spatial frequencies is determined by only 3 parameters, namely the displacements. Therefore, the displacements can be derived using a least squares estimate as

$$\Delta\vec{r} = K^{-1}\Delta\vec{\phi}, \tag{3}$$

where K^{-1} is the pseudo-inverse of matrix K.

In the context of 3D vector flow imaging, we want to know the velocity at various parts of the image. In order to do so, equation (3) can be applied to multiple beamformed sub-volumes that may be partially overlapping. We will be using beamformed RF data as input, but IQ or envelope data works as well. To prevent artefacts due to edge effects, the sub-volumes are windowed before the applying the Fourier Transform. Like Lenge *et al.* we have used a Hann window for this. After the displacements have been calculated, the velocities can be retrieved by dividing the displacements by the frame interval.

The presented algorithm is most similar to a phase-correlation algorithm that first applies the correlation via the Fourier domain and then does the peak-finding in the spatial domain. The algorithm presented in this proceeding skips the inverse transform and peak-finding, and instead derives the displacements directly from the phase characteristics in the Fourier domain. The main advantage is a reduction in computational complexity.

B. Choice of frequencies

In the absence of noise, clutter and aliasing, three combinations of frequencies could provide a unique solution for the velocities. In case things are not as ideal, more frequency sets have to be used to increase the accuracy. A possible choice for RF data as given by Lenge *et al.* is to choose a set of lateral spatial frequencies (k_x, k_y) that are equally spaced over the whole frequency band. The axial frequencies are chosen to cover a limited bandwidth around the central frequency $k_{z,0}$, which is related to the centre frequency f_0 of the received signal.

The above choice of frequencies works well for most situations, but it can be improved. Frequencies that have a low magnitude are susceptible to the effects of noise, clutter and aliasing due to spatial undersampling. Therefore, it is better to exclude frequencies with a low magnitude from the estimation, as also done by Stone *et al.* [11].

The phase difference between two frames is only unambiguous over the range $\pm\pi$. This range is exceeded in 1D for the highest spatial frequency in the Fourier domain if the displacement is larger than a grid step. In 2D and 3D, this happens for the highest spatial frequencies if the L^1 norm of the displacements relative to the grid steps exceeds 1. Therefore, to prevent aliasing due to large displacements, the frequencies used for estimating the displacement should satisfy

$$\frac{k_x}{k_{x,\max}} + \frac{k_y}{k_{y,\max}} + \frac{k_z}{k_{z,\max}} \leq 1 \tag{4}$$

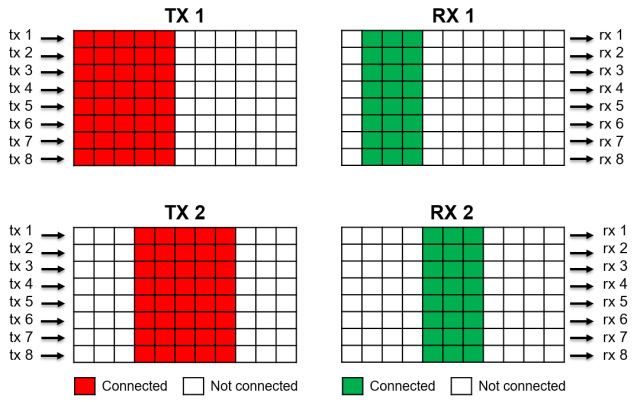

Fig. 1. Illustration of the imaging scheme. In this case the transmit and receive apertures are respectively 5 and 3 columns wide and the aperture is translated by 3 columns after each shot.

where $(k_{x,\max}, k_{y,\max}, k_{z,\max})$ are chosen depending on the maximum expected displacement in each direction. For example, if the expected displacement in a certain direction is two times the grid step, then the maximum frequency in that direction should be half the Nyquist frequency.

III. Experimental setup

A. Flow phantom

The flow phantom consisted of a water-enclosed heat-shrink tube with a diameter of 6.4 mm. The tube was centred at about 16 mm from the probe and the main direction of flow was in the row (y) direction of the probe, which is similar to the envisaged orientation of the matrix probe on the carotid. There was no long tube before the measurement area, so a parabolic flow cannot be ensured. Through the tube we pumped a blood-mimicking fluid (chocolate milk) using a centrifugal pump (Classic 2211, Eheim GmbH & Co. KG, Deizisau, Germany). As a reference for the average flow velocity, an ultrasonic flow meter (Flownetix 107, Flownetix Limited, Birmingham, UK) was used. The measured flow rate using this meter was about 7.75 ml s^{-1} during the measurement, translating to an average velocity of 24 cm s^{-1}.

B. Matrix transducer

We used a prototype PZT-on-ASIC matrix transducer designed for imaging the carotid bifurcation [7]. The prototype consists of 3840 elements subdivided in 80 columns and 48 rows. The element pitch is 150 µm × 300 µm and the centre frequency is about 7.5 MHz. The final version of this matrix transducer will contain 120 rows instead of the current 48 and will thus be more than twice as large.

C. Acquisition and beamforming

A major issue with large matrix transducer is connecting the enormous amount of elements. This matrix transducer has a single input and output per row, reducing the channel count by a factor of 80. This is different compared to a row-column matrix array which has its inputs and outputs oriented orthogonally.

Due to the row-based architecture of our matrix array, it operates like an electronically translatable linear array. During each transmit/receive event, a subset of the columns is used and for the next event the columns are translated. An example is shown in Fig. 1.

In our measurements an image was constructed from 9 of these events. In transmit, a sub-aperture of 15 columns was used and in receive, a sub-aperture of 5 columns was employed. This sub-aperture was translated by 5 columns after every shot. With this scheme we achieved a frame rate of 1.8 kHz.

Beamforming was performed offline using a Fourier domain method [8]. After beamforming, the images were upsampled by a factor of 3 and 2 in respectively the column and the row direction with respect to the pitch of the used elements. The upsampling was done by zero-padding in the frequency domain. Finally, to remove the tube signal from the images, the mean of the previous 20 frames was subtracted from each image.

D. Velocity estimation parameters

For the estimation we subdivided the image into overlapping blocks of 2.5 mm $\times$ 6 mm $\times$ 2.5 mm with a spacing of 0.5 mm in all directions between the centres of the blocks. The number of unique frequencies in each direction was respectively 5, 8 and 6. The used frequencies were equally spaced within the band given by equation (4) and within a bandwidth equivalent to 6 MHz around the centre frequency in the axial direction. Finally, the maximum frequency in the y-direction was limited to ensure that measuring 48 cm s^{-1} was possible, which is the maximum expected velocity assuming a parabolic flow. These settings resulted in 33 combinations of frequencies being used for the estimation.

IV. Results

Fig. 2 shows the measured velocity profile, averaged over all 340 frames. It is consistent with the direction of applied flow and the shape of the tube in the measurement area. Looking at the overall flow profile, the shape appears plausible with the highest velocity at the centre and a decrease in velocity towards the edges. However, we do not know what the exact flow profile should be as there is no long entrance tube before the measurement area to ensure a parabolic flow profile.

Looking more closely at the profile, it can be seen that the profile is not exactly circularly symmetric. There are two main reasons for this. First, the tube itself is not completely round. This can be noted by observing that the top and bottom of the tube, the only parts that are expected to be visible, appear at a different x-position. Second, due to the long pulse length and large effective pitch in the x-direction, the resolution in x and z is poor. This causes a spread of velocities in the sample volume, resulting in an underestimation of the actual velocity [10].

The maximum velocity in the shown profile is 27.2 cm s^{-1}. Compared to the average velocity as measured by the flow meter, which was about 24 cm s^{-1}, this maximum is relatively low. With a parabolic flow the maximum should have been about 48 cm s^{-1}. Although we don't expect to have a parabolic flow, we still would have expected a higher maximum velocity.

The reason for the relatively low maximum velocity after averaging can be found by looking at the velocity over time as shown Fig. 3. The top panel shows the velocity measured at $(0, 0.5, 15.5)$ mm and the bottom panel the velocity measured at $(0, 2, 16.5)$ mm. Both points are in the central part of the measurement area. The figure shows that the measured velocity varies significantly over time. Interestingly, the estimated velocity is periodic with a period of 90 ms. We therefore expect that the pump is the main cause for the large variation in estimated velocity.

V. Discussion

The results show that we can estimate a volumetric velocity profile using our matrix transducer and the proposed algorithm with the correct order of magnitude and direction. To improve the results and show that the estimated velocity is accurate, we first have to solve several issues related to the transducer, acquisition and flow phantom which we discuss in the paragraphs below.

There are two main issues with the current prototype. First, the pitch in the row direction is 300 µm, which translates to 1.5 λ. The most prominent effect of this very large pitch is an increased amount of internal element ringing that deteriorates the axial resolution [12]. Second, an ASIC is not a good backing as it has a poor attenuation. Therefore, Lamb waves can propagate in the ASIC and cause cross-talk between the elements. This negatively affects the directivity and increases the amount of ringing [13].

The issue with the acquisition is that it is not possible to achieve a high frame rate, high resolution, high contrast and a wide imaging volume in the column direction all at the same time. The current imaging scheme requires multiple transmit/receive events to construct a single frame. To achieve the frame rate high the amount of shots per frame is limited. In our case 9 shots were used and with this we achieved a frame rate of 1.8 kHz. In order to still achieve a decent resolution and imaging volume in the column direction of the probe, the effective element width was increased to 5 columns, which resulted in an aperture width of 6.75 mm. The main downside of this approach is that the large pitch results in severe grating lobes. We reduced the negative effects of this by reducing the Tx aperture in the column direction and using a Fourier domain beamformer [8], which proved to be more effective than a DAS beamformer in our case.

The used flow phantom does not include a long entrance tube and does not have an exactly round tube in the measurement volume. Therefore, we are not able to compare the measured flow profile with a ground truth. Another issue is that the pump is not able to provide a constant flow velocity as indicated by Fig. 3. Instead, the velocity appears to vary periodically with a period of 90 ms.

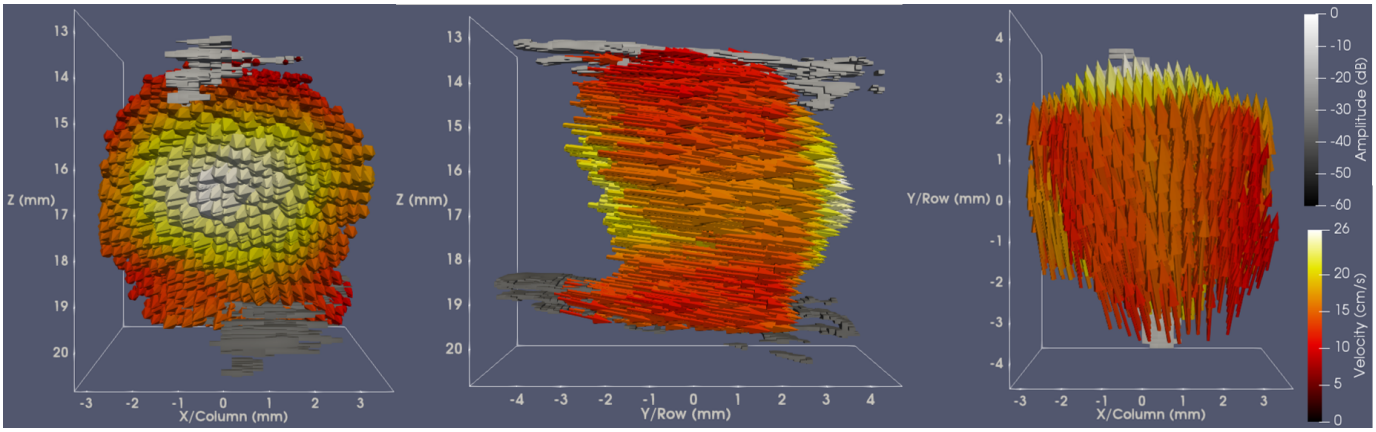

Fig. 2. Front, side and bottom view of the averaged velocity profile in the tube.

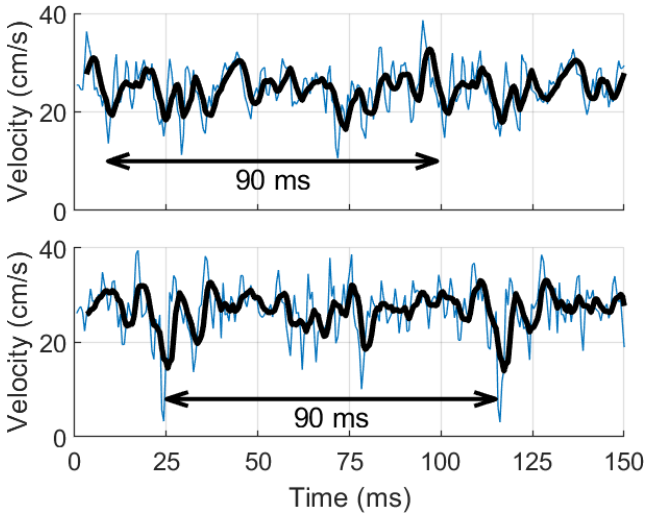

Fig. 3. Velocity over time at two points in the measurement volume. In blue the raw velocity and in black the velocity averaged over the last 5 frames.

VI. Conclusion

In this proceeding we have shown the first full-volume 3D vector flow imaging results as obtained with our matrix array. We also extended a frequency domain vector flow imaging to 3D. The obtained direction and magnitude of the velocity are in qualitative agreement with the expectations. These results indicate that it is feasible to estimate 3D velocity vectors on a 3D grid using our matrix transducer and the proposed algorithm.

Acknowledgement

This research is part of the project 'Monitoring infant brain perfusion by trans-fontanel echography (MIFFY)' with project number 15293, which is (partly) financed by the Netherlands Organization for Scientific Research (NWO).

References

[1] I. Kallikazaros, C. Tsioufis, S. Sideris, C. Stefanadis, and P. Toutouzas, "Carotid artery disease as a marker for the presence of severe coronary artery disease in patients evaluated for chest pain," *Stroke*, vol. 30, no. 5, pp. 1002–1007, 1999.

[2] A. Harloff, "Carotid Plaque Hemodynamics," *Interventional Neurology*, vol. 1, no. 1, pp. 44–54, 2012.

[3] P. Kruizinga, F. Mastik, J. G. Bosch, A. F. Van Der Steen, and N. De Jong, "Carotid artery wall dynamics captured with multi-plane high-frame-rate imaging," *2015 IEEE International Ultrasonics Symposium, IUS 2015*, 2015.

[4] M. Couade, M. Pernot, E. Messas, J. Emmerich, A. Hagège, M. Fink, and M. Tanter, "Ultrafast imaging of the arterial pulse wave," *Irbm*, vol. 32, no. 2, pp. 106–108, 2011.

[5] A. Ramalli, E. Boni, A. S. Savoia, and P. Tortoli, "Density-tapered spiral arrays for ultrasound 3-D imaging," *IEEE Transactions on Ultrasonics, Ferroelectrics, and Frequency Control*, vol. 62, no. 8, pp. 1580–1588, 2015.

[6] C. E. Morton and G. R. Lockwood, "Theoretical assessment of a crossed electrode 2-D array for 3-D imaging," *Proceedings of the IEEE Ultrasonics Symposium*, vol. 1, no. c, pp. 968–971, 2003.

[7] E. Kang, Q. Ding, M. Shabanimotlagh, P. Kruizinga, Z. Y. Chang, E. Noothout, H. J. Vos, J. G. Bosch, M. D. Verweij, N. De Jong, and M. A. Pertijs, "A Reconfigurable Ultrasound Transceiver ASIC With 24 × 40 Elements for 3-D Carotid Artery Imaging," *IEEE Journal of Solid-State Circuits*, vol. 53, no. 7, pp. 2065–2075, 2018.

[8] J. Y. Lu, "2D and 3D High Frame Rate Imaging with Limited Diffraction Beams," *IEEE Transactions on Ultrasonics, Ferroelectrics, and Frequency Control*, vol. 44, no. 4, pp. 839–856, 1997.

[9] L. Merabet, S. Robert, and C. Prada, "2-D and 3-D Reconstruction Algorithms in the Fourier Domain for Plane-Wave Imaging in Non-destructive Testing," *IEEE Transactions on Ultrasonics, Ferroelectrics, and Frequency Control*, vol. 66, no. 4, pp. 772–788, 2019.

[10] M. Lenge, A. Ramalli, E. Boni, H. Liebgott, C. Cachard, and P. Tortoli, "High-frame-rate 2-D vector blood flow imaging in the frequency domain," *IEEE transactions on ultrasonics, ferroelectrics, and frequency control*, vol. 61, no. 9, pp. 1504–1514, 2014.

[11] H. S. Stone, M. T. Orchard, E. C. Chang, and S. A. Martucci, "A fast direct Fourier-based algorithm for subpixel registration of images," *IEEE Transactions on Geoscience and Remote Sensing*, vol. 39, no. 10, pp. 2235–2243, 2001.

[12] J. Janjic, M. Shabanimotlagh, G. van Soest, A. F. W. van der Steen, N. de Jong, and M. D. Verweij, "Improving the Performance of a 1-D Ultrasound Transducer Array by Subdicing," *IEEE Transactions on Ultrasonics, Ferroelectrics, and Frequency Control*, vol. 63, no. 8, pp. 1161–1171, 2016.

[13] M. Shabanimotlagh, V. Daeichin, S. B. Raghunathan, P. Kruizinga, H. J. Vos, J. G. Bosch, M. Pertijs, N. De Jong, and M. Verweij, "Optimizing the directivity of piezoelectric matrix transducer elements mounted on an ASIC," *IEEE International Ultrasonics Symposium, IUS*, 2017.